

Hubbard interactions in iron-based pnictides and chalcogenides: Slater parametrization, screening channels and frequency dependence

Ambroise van Roekeghem,^{1,2} Loïc Vaugier,¹ Hong Jiang,³ and Silke Biermann^{1,4}

¹*Centre de Physique Théorique, Ecole Polytechnique,
CNRS UMR 7644, Université Paris-Saclay, 91128 Palaiseau, France*

²*Beijing National Laboratory for Condensed Matter Physics,
and Institute of Physics, Chinese Academy of Sciences, Beijing 100190, China **

³*College of Chemistry and Molecular Engineering, Peking University, 100871 Beijing, China*

⁴*Collège de France, 11 place Marcelin Berthelot, 75005 Paris, France*

(Dated: today)

We calculate the strength of the frequency-dependent on-site electronic interactions in the iron pnictides LaFeAsO, BaFe₂As₂, BaRu₂As₂, and LiFeAs and the chalcogenide FeSe from first-principles within the constrained random phase approximation. We discuss the accuracy of an atomic-like parametrization of the two-index density-density interaction matrices based on the calculation of an optimal set of three independent Slater integrals, assuming that the angular part of the Fe-*d* localized orbitals can be described within spherical harmonics as for isolated Fe atoms. We show that its quality depends on the ligand-metal bonding character rather than on the dimensionality of the lattice: it is excellent for ionic-like Fe-Se (FeSe) chalcogenides and a more severe approximation for more covalent Fe-As (LaFeAsO, BaFe₂As₂) pnictides. We furthermore analyze the relative importance of different screening channels, with similar conclusions for the different pnictides but a somewhat different picture for the benchmark oxide SrVO₃: the ligand channel does not appear to be dominant in the pnictides, while oxygen screening is the most important process in the oxide. Finally, we analyze the frequency dependence of the interaction. In contrast to simple oxides, in iron pnictides its functional form cannot be simply modeled by a single plasmon, and the actual density of modes enters the construction of an effective Hamiltonian determining the low-energy properties.

PACS numbers: 71.27.+a, 71.10.Fd, 71.15.Ap, 71.45.Gm

I. INTRODUCTION

The discovery of unconventional superconductivity with critical temperatures up to 55 K in iron-based pnictides and chalcogenides has raised tremendous interest in the electronic properties of the various classes of these materials (for recent reviews, see 1–3). The first prototypes were LaFeAsO^{4–8}, representing the “1111” family and the “122” compound BaFe₂As₂^{9–11}. Soon, however, also the “111” stoichiometry (such as in LiFeAs^{12–14}), and the “11” chalcogenides FeSe and FeTe^{15–17}) got into the spotlight.

While an obvious difference to the high-temperature superconducting cuprates is the metallic nature of the undoped iron-pnictides, this observation does not *a priori* justify a weak-coupling approach, and several recent works^{18,19} suggest a possibly much closer connection to the cuprates than anticipated. Quite generically, most iron pnictide compounds exhibit magnetically ordered phases in close proximity to the superconducting ones, and the relation between the former and the latter remains an open question. Early models based on a strong coupling picture have met some success in describing the nature of magnetic ordering, when invoking a biquadratic exchange term²⁰.

On the other hand, early on, a puzzle concerning the value of the measured magnetic moments was pointed out, namely a magnetic moment much smaller than the

one expected from a high spin configuration for the Fe 3*d* shell, or from density functional theory (DFT) calculations^{21,22}. Within a purely local picture, the large Hund’s coupling, dominating over crystal and ligand field splittings, would be expected to induce a high-spin configuration. LaFeAsO, for example, exhibits an antiferromagnetic local moment between 0.3 – 0.6 μ_B below $T \sim 130$ K^{23,24}, much smaller than the magnetic moment calculated within DFT (2 μ_B). This anomaly was interpreted as a solvation effect due to the extremely large polarisability of the arsenic ligands²⁵, which leads to a strong reduction of the Hubbard interaction on the Fe *d* manifold. In “122” and in “11” families, on the other hand, larger magnetic moments were determined: around 0.9 μ_B for BaFe₂As₂²⁶ and 2.2 μ_B for FeTe²⁷. Recent calculations of two-particle correlation functions within local density approximation (LDA) combined with dynamical mean field theory (DMFT) have rather suggested dynamic quantum fluctuations to be the origin of these puzzles, inducing a “dichotomy” between large local but small ordered magnetic moments as measured within neutron experiments^{28,29}. Yet another example where the timescale of the experimental probe is decisive for the outcome of a measurement was recently also analyzed in Ref. 30.

Determining the strength of electronic Coulomb correlations appears therefore an important issue not only for understanding their role for electronic, magnetic and transport properties but even for establishing the frame-

work and language in which those are best described.

An additional difficulty arises from a particularity of the iron pnictides, which – due to their closeness to a filling of 6 electrons in 5 orbitals and substantial Hund’s rule coupling – exhibit an extreme sensitivity with respect to small changes in parameters, and compounds with moderate electronic correlations can be tuned into rather strongly correlated ones by modest changes in interaction strength, in particular Hund’s coupling, doping, or composition.

To address such questions, it is mandatory to construct realistic Hamiltonians to which many-body tools can be applied. The discovery of the iron pnictides has thus opened an important new testbed for *ab initio* techniques for correlated materials. Even when restricting to dynamical mean field theory-based calculations^{31–34}, the early literature is abundant^{35–43}. Many of the early works were based on one-particle Hamiltonians derived from density functional theory, supplemented by many-body interaction terms which were taken as adjustable parameters. It became soon clear, however, that this is an insufficient strategy for a truly materials-specific description of iron-pnictides. The determination – from first principles – of the effective local Coulomb interactions is therefore an important intermediate goal for quantitative theories of iron pnictides.

A most promising route is the constrained random phase approximation (cRPA)⁴⁴ – an approach for deriving from first-principles the interacting Hamiltonian within a target subspace that is appropriate for describing the low-energy many-body properties (“downfolding”). Refs. [38,42,45–55] demonstrated the usefulness of the cRPA for iron pnictides. For LaFeAsO, Ref. [38] considered a Hubbard Hamiltonian (dubbed “*d-dp*”) that incorporated both, Fe 3*d* and ligand As and O *p* states as degrees of freedom, but with a Coulomb energy cost on Fe 3*d* orbitals only. The effective interactions for this specific low-energy model were calculated within the cRPA⁴⁴, and the many-body Hamiltonian was solved within LDA+DMFT. Within this scheme, LaFeAsO was described as a metal with moderate strength of the electronic correlations³⁸, whereas the largest effects were found for α -FeSe⁴² in agreement with recent photoemission experiments^{56,57}. In addition, Hund’s rule coupling, *J*, appeared to play a fundamental role in the description of the low-energy properties of FeSe, as also noted by Haule and co-workers⁴⁰ for characterizing the coherence-incoherence crossover temperature in LaFeAsO.

Beyond giving first principles estimates for the effective Hubbard and Hund’s interactions for specific materials calculations, the cRPA enables systematic studies of trends along the series. In this way, the larger values of *U* and *J* in the chalcogenides as compared to the pnictides were rationalized⁴⁶, based on their electronic structure.

The interpretation of the effective local Hubbard interaction as *partially screened* interaction, that underlies the cRPA strategy has an interesting further consequence: since screening is a dynamical process, the partially

screened interactions *U* and *J* are also dynamical, that is, frequency-dependent quantities⁵⁸. The impact of this energy-dependence on the low-energy properties and the coupling between electronic and plasmonic excitations in many-body calculations has been studied recently in prototypical models and the benchmark oxide SrVO₃^{59–61} as well as in several transition metal pnictides^{51,52,55}. The inclusion of energy-dependent Hubbard interactions within an extended version of LDA+DMFT^{55,59} leads to a reduction of the quasi-particle weight at the Fermi energy, compared to standard many-body techniques, e.g. LDA+DMFT. The spectral weight is shifted to additional satellites at larger energies, in good agreement with photoemission experiments. A systematic procedure for constructing low-energy Hamiltonians that incorporate both, an interacting Hamiltonian downfolded into a low-energy subspace, and the renormalization of the one-particle part of the Hamiltonian due to electron-plasmon excitations, was introduced in Ref. [47]. It consists in estimating from *U*(ω), a plasmon coefficient that reduces the kinetic energy. The values of such coefficients are between 0.59 and 0.63 for LaFeAsO, FeSe and BaFe₂As₂⁴⁷.

In this paper, the strength of the frequency-dependent on-site electronic interactions in the iron-based pnictide (LaFeAsO, BaFe₂As₂ and BaRu₂As₂, LiFeAs) and chalcogenide (FeSe) families is calculated from first-principles within the cRPA⁴⁴. We use the recent implementation of Ref. [62], based on the electronic structure code Wien2k⁶³. Both Fe *d* and ligand As (and O in oxypnictides) *p* degrees of freedom are considered in the construction of the resulting parameter-free low-energy “*dp-dp*” Hamiltonian. An effective “*d-dp*” Hamiltonian where only the occupation on Fe-*d* orbitals is affected by the Coulomb repulsion can then be constructed via the recently proposed “shell-folding” procedure⁶⁴ that we extend here to the frequency-dependent case. The results of this scheme for the static value of the interaction parameter are similar to calculations in a *d-dp* model in which only the transitions from and to the bands with a majority of *d*-orbital character are cut within constrained-RPA and *U*_{*dp*} is neglected⁴⁹. On the other hand, the infinite frequency value is reduced by about 30%. In agreement with the literature, we find in Section III that the effective Coulomb interactions for Fe-3*d* shells, are larger in “11” chalcogenides than in “122” and “1111” pnictides, while the “111” are an intermediate case.

The accuracy of an atomic-like parametrization of the two-index density-density interaction matrices within the “*dp-dp*” low-energy Hamiltonian is discussed in Section III. It is based on the calculation of an optimal set of three independent Slater integrals, assuming that the angular part of the Fe-*d* localized orbitals can be described within spherical harmonics as for isolated Fe atoms (see Section II for an introduction). We find that the accuracy of this parametrisation depends on the ligand-metal bonding character rather than on the dimensionality of the lattice: it is excellent for ionic-like Fe-Se (FeSe)

chalcogenides and less appropriate for more covalent Fe-As (LaFeAsO, BaFe₂As₂) pnictides. This illustrates the differences in the sphericity of the Fe-3*d* Wannier orbitals and in the anisotropy of the screening.

In Section IV, we investigate the relative importance of screening channels which reduce the on-site bare interaction to the fully screened one. We show that the screening channels are analogously structured in the pnictide and chalcogenide families, while this structure is very different in a benchmark oxide, namely SrVO₃. The ligand channel does not appear to be responsible for the dominant screening mechanism in iron pnictides.

Finally, we analyze the frequency dependence of the interaction and its relation with the values of the free-electron plasmon frequencies in Section V. In contrast to simple oxides, in iron pnictides its functional form cannot be simply modeled with a single plasmon, and the actual density of modes enters the construction of the effective Hamiltonian determining the low-energy properties, through a renormalisation of the quasiparticle dispersions.

II. METHOD

A. General framework

The cRPA⁴⁴ is a first principles tool to construct low-energy Hamiltonians with specific “target” degrees of freedom. The main idea consists in identifying Hubbard and Hund’s interactions with matrix elements of a partially screened interaction W^r within a set of localized Wannier(-like) orbitals $\{|\phi_m\rangle\}$, with m an orbital quantum number. The partially screened interaction W^r corresponds to the bare Coulomb interaction within the target low-energy subspace for which explicit many-body calculations are carried out. Within the full Hilbert space W^r is a partially screened interaction, screened by higher energy degrees of freedom not included in the target space. The most straightforward option is to choose as the target space the space spanned by the functions $\{|\phi_m\rangle\}$ but other options are possible and will be exploited below.

The partially screened interaction W^r is calculated by constraining the polarization such that the screening processes involving the target states included in the low-energy Hamiltonian are not double counted in a further many-body calculation. The random phase approximation gives an explicit expression for the polarization, P , in terms of transitions between occupied and empty states. Within this assumption, it is possible to calculate the constrained polarization $P^r = P - P^{sub}$, where P^{sub} is the polarization within the target low-energy subspace only⁶². It is energy-dependent since screening is a dynamical process. W^r is defined as the interaction screened by P^r :

$$W_r = [1 - vP_r]^{-1}v \quad (1)$$

The additional screening taking place in the low-energy subspace then allows us to recover the fully screened interaction W :

$$\begin{aligned} W &= [1 - vP]^{-1}v = [1 - vP^r - vP^{sub}]v \\ &= \frac{v/[1 - vP^r]}{1 - [v/[1 - P^rv]]P^{sub}} \\ &= [1 - W^rP^{sub}]^{-1}W^r \end{aligned} \quad (2)$$

B. Interaction matrices

The value of the partially screened interaction W^r between local orbitals is expressed in terms of the four-index interaction matrix $U_{m_1m_2m_3m_4}^{(S)}$:

$$\begin{aligned} U_{m_1m_2m_3m_4}^{(S)}(\omega) &\equiv \langle \phi_{m_1}\phi_{m_2}|W^r(\omega)|\phi_{m_3}\phi_{m_4}\rangle \\ &= \iint d^3rd^3r' \phi_{m_1}^*(r)\phi_{m_3}(r)W^r(r,r';\omega)\phi_{m_2}^*(r')\phi_{m_4}(r') \end{aligned} \quad (3)$$

where the superscript S is added for specifying the angular symmetry of the localized orbitals considered.

Most matrix elements are of the order of 0.1 eV or less, except for two-index reduced interaction matrices, $U_{mm'}^{\sigma\sigma}|_{\text{cRPA}}$, $U_{mm'}^{\sigma\bar{\sigma}}|_{\text{cRPA}}$ and $J_{mm'}^{\text{cubic}}$ which can be extracted from the calculation. Cubic angular harmonics are considered in our case as an approximation to the crystal field in the iron-based pnictides and chalcogenides:

$$U_{mm'}^{\sigma\bar{\sigma}}|_{\text{cRPA}} \equiv U_{mm'mm'}^{\text{cubic}} = \langle \phi_m\phi_{m'}|W^r(0)|\phi_m\phi_{m'}\rangle \quad (4)$$

$$U_{mm'}^{\sigma\sigma}|_{\text{cRPA}} \equiv U_{mm'mm'}^{\text{cubic}} - U_{mm'm'm}^{\text{cubic}} \quad (5)$$

where m runs over the d orbital subspace and σ refers to the spin degree of freedom.

As two atoms of Fe are found in the conventional unit-cell of the iron-based pnictides and chalcogenides, one has access to the nearest-neighbor interaction between Fe-3*d* orbitals within equation 3 (see Ref. [62] for a more general expression of the non-local interactions). One can also calculate the interaction between Fe-3*d* and As-4*p* orbitals in the same way.

C. Slater parametrization

Replacing the four-index interaction matrix $U_{m_1m_2m_3m_4}$ by a small subset of fitting parameters is usually done in the literature of many-body calculations, e.g. LDA+U or LDA+DMFT, in order to avoid double-counting issues. However, the errors induced by considering such an approximated interacting Hamiltonian in many-body calculations have not been investigated yet⁸². For isolated atoms, the development into a finite number of Legendre polynomials of the matrix elements of the Coulomb potential with

spherical harmonics is exact^{65–67}. It involves only three radial integrals – or Slater integrals – for d states, whereas the angular part is determined with well defined Racah-Wigner coefficients, α_k :

$$\alpha_k(m_1, m_2, m_3, m_4) = \frac{4\pi}{2k+1} \sum_{q=-k}^k \langle Y_{lm_1} | Y_{kq} Y_{lm_3} \rangle \langle Y_{lm_2} Y_{kq} | Y_{lm_4} \rangle \quad (6)$$

where Y_{lm} are spherical harmonics and $\langle Y_{l_1 m_1} | Y_{l_2 m_2} Y_{l_3 m_3} \rangle$ refer to the Gaunt coefficients. It is the sphericity of the isolated atom – and of the spherical harmonics used – that sets the finite number of the Slater integrals to $l+1$ where l is the orbital quantum number.

Assuming that i) the localized Wannier orbitals, $\{|\phi_{m,-2 \leq m \leq 2}\rangle\}$, to which the Hamiltonian is downfolded at low-energy, still retain the sphericity of the isolated atom although they are embedded in the solid, and ii) screening does not induce strong orbital anisotropy, allows to define Slater integrals for correlated orbitals in materials as follows⁶²:

$$F^k(\omega) = \mathcal{C}_{l,k} \sum_{m_1, m_2, m_3, m_4} (-1)^{m_1+m_4} U_{m_1 m_2 m_3 m_4}^{(\text{spheric})}(\omega) \times \begin{pmatrix} l & k & l \\ -m_1 & m_1 - m_3 & m_3 \end{pmatrix} \begin{pmatrix} l & k & l \\ -m_2 & m_2 - m_4 & m_4 \end{pmatrix} \quad (7)$$

where the parentheses correspond to the Wigner 3j-symbols and the coefficients $\mathcal{C}_{l,k}$ are defined as follows:

$$\mathcal{C}_{l,k} = \frac{2k+1}{(2l+1)^2 \begin{pmatrix} l & k & l \\ 0 & 0 & 0 \end{pmatrix}^2}. \quad (8)$$

The superscript “spheric” indicates that Wannier orbitals with spherical angular harmonics are employed. The usual definition of the Hubbard $U = F^0$ and Hund’s exchange $J = (F^2 + F^4)/14$ follows. Analogously, we define the bare parameters, v and J_{bare} when considering the Slater integrals that parametrize the bare interaction matrix elements.

The Slater integrals can be used for calculating the Slater-symmetrized interaction matrix, $\bar{U}_{m_1 m_2 m_3 m_4}^{(\mathcal{S})}$, with the symmetry \mathcal{S} of the crystal field:

$$U_{m_1 m_2 m_3 m_4}^{(\mathcal{S})}(\omega) = \sum_{m'_1 m'_2 m'_3 m'_4} \mathcal{S}_{m_1 m'_1} \mathcal{S}_{m_2 m'_2} \times \left\{ \sum_{k=0}^{2l} \alpha_k(m'_1, m'_2, m'_3, m'_4) F^k(\omega) \right\} \mathcal{S}_{m'_3 m_3}^{-1} \mathcal{S}_{m'_4 m_4}^{-1} \quad (9)$$

Choosing \mathcal{S} as the transformation from spherical to cubic harmonics leads to the Slater-symmetrized reduced interaction matrices with cubic symmetry:

$$\bar{U}_{mm'}^{\sigma\bar{\sigma}}|_{\text{Slater}} \equiv \bar{U}_{mm'mm'}^{\text{cubic}} \quad (10)$$

$$\bar{U}_{mm'}^{\sigma\sigma}|_{\text{Slater}} \equiv \bar{U}_{mm'mm'}^{\text{cubic}} - \bar{U}_{mm'm'm}^{\text{cubic}}. \quad (11)$$

We stress that within this method three independent Slater integrals are deduced for d Hubbard interaction matrices, see Ref. [49] for details. This allows for an unbiased check of the commonly used assumption of setting the ratio F^4/F^2 to a fixed value of 0.63 for 3d orbitals, leaving only two independent Slater integrals (see e.g. the discussion in⁶⁸). Relations similar to equation 7 were used in Ref. [69] for BaFe₂As₂, based on a self-consistent GW approximation for calculating the four-index Hubbard interaction matrix.

D. Frequency dependence

Because of the frequency dependence of the constrained polarization, the partially screened interaction W^r is also frequency dependent. Consequently, the U matrix and the Slater integrals parametrizing it are defined as a function of frequency: $U = U(\omega)$. At infinite frequency, the interaction $W^r(\omega = \infty)$ is equal to the bare, unscreened Coulomb interaction v . The largest variation is observed on the monopole part F_0 , which can be reduced by one order of magnitude at zero frequency compared to the unscreened value, while the multipole terms are proportionally less impacted^{70–72}.

Naively, one might think that the high-frequency tail should have little influence on the low-energy spectral properties, since typical plasmon frequencies are usually the largest energy scale in the problem. This is however not true, due to the mechanism alluded to above: the frequency-dependence can be understood as resulting from a coupling of the electrons to bosonic screening degrees of freedom, and the resulting eigenstates of the coupled fermion-boson problem can be understood as “electronic polarons”, electrons dressed by their bosonic screening cloud. These entities have larger effective masses and thus renormalised dispersions. An explicit construction of an effective low-energy Hamiltonian incorporating these renormalisation has been derived in Ref. 47. The idea is to introduce a bosonic renormalization factor Z_B accounting for the screening modes⁴⁷. In the general form for the dynamical interaction $\frac{1}{2} (V\delta(\tau) + U_{\text{ret}}(\tau)) n(\tau)n(\tau')$, the screening is contained in U_{ret} while V corresponds to the bare interaction. Introducing the screening modes of energy ω and coupling strength $\lambda(\omega) = \sqrt{-\Im(U_{\text{ret}}(\omega))/\pi}$ allows us to parametrize U_{ret} as:

$$U_{\text{ret}}(\tau) = - \int_0^\infty d\omega \lambda^2(\omega) \cosh \left[\left(\tau - \frac{\beta}{2} \right) \omega \right] / \sinh \left[\frac{\beta\omega}{2} \right] \quad (12)$$

and we can then write the Hamiltonian as a Hubbard-

Holstein model:

$$\begin{aligned}
H = & - \sum_{ij\sigma} t_{ij} d_{i\sigma}^\dagger d_{j\sigma} + V \sum_i d_{i\uparrow}^\dagger d_{i\uparrow} d_{i\downarrow}^\dagger d_{i\downarrow} + \mu \sum_{i\sigma} d_{i\sigma}^\dagger d_{i\sigma} \\
& + \int_0^\infty \omega \sum_i b_i^\dagger(\omega) b_i(\omega) d\omega \\
& + \int_0^\infty \lambda(\omega) \sum_{i\sigma} d_{i\sigma}^\dagger d_{i\sigma} \left(b_i(\omega) + b_i^\dagger(\omega) \right) d\omega \quad (13)
\end{aligned}$$

where i, j are the index of the lattice sites, t_{ij} is the hopping amplitude between sites i and j , μ the chemical potential of the system, $d_{i\sigma}^\dagger$ ($d_{i\sigma}$) the creation (annihilation) operator of electrons of spin σ on site i and $b_i^\dagger(\omega)$ ($b_i(\omega)$) the creation (annihilation) operator of a quantum of energy in the bosonic mode of energy ω .

Applying a generalized Lang-Firsov transformation to the model^{73,74} and projecting onto the subspace of zero-boson states (an approximation valid at low energies) finally provides us with the following Hamiltonian:

$$H_{eff} = - \sum_{ij\sigma} Z_B t_{ij} d_{i\sigma}^\dagger d_{j\sigma} + U_0 \sum_i d_{i\uparrow}^\dagger d_{i\uparrow} d_{i\downarrow}^\dagger d_{i\downarrow} \quad (14)$$

Where U_0 is the static value of the Coulomb interaction and Z_B reflects the density of screening modes $\frac{\Im U_{ret}(\omega)}{\pi\omega^2}$:

$$\ln(Z_B) = - \int_0^{+\infty} \frac{\Im U_{ret}(\omega)}{\pi\omega^2} d\omega \quad (15)$$

Physically, it implies that at low energy the spectral function is further renormalized by Z_B , and the remaining weight is transferred to higher energy. Moreover, the hopping amplitude between non-correlated and correlated states will be reduced by a factor $\sqrt{Z_B}$.

E. Shell-folding

At infinite frequency screening is suppressed and the instantaneous intrashell Coulomb interaction in iron pnictides, $U^{dd}(\omega = \infty)$, is around 20 eV. This is about one order of magnitude bigger than the static interaction $U^{dd}(\omega = 0)$. At the same time, the intershell p - d interaction $U^{dp}(\omega = \infty)$ is of the order of 6 eV, and it would seem unreasonable to neglect it. Indeed, the pd -interaction can provide an important screening mechanism, since adding charge on the d -shell can push charge out of the p -shell, thus reducing the electron addition cost. This mechanism is familiar since the early ideas of Herring⁷⁵ on “perfect screening”. As discussed recently⁶⁴, in the context of the cRPA it can be used to construct a “shell-folding” scheme that allows to include pd -screening even in situations where entanglement between d - and p -states makes the standard “ d - dp ” procedure of the cRPA ill-defined. We briefly review the main idea, since in the later sections we will give results

both using the standard procedure and the shell-folded scheme. In particular, we will use an extended version of shell-folding in the frequency-dependent case.

The main idea can be understood by considering the following purely algebraic manipulation: We start from a dp model, where the interaction part of the Hamiltonian on one site reads:

$$\begin{aligned}
H_{int} = & \frac{1}{2} \sum_{\substack{(m,\sigma) \neq (m',\sigma') \\ m,m' \in \{d\}}} U_{m\sigma m'\sigma'}^{dd} n_{m\sigma} n_{m'\sigma'} \\
& + \frac{1}{2} \sum_{\substack{(m,\sigma) \neq (m',\sigma') \\ m,m' \in \{p\}}} U_{m\sigma m'\sigma'}^{pp} n_{m\sigma} n_{m'\sigma'} \\
& + \sum_{\sigma,\sigma'} U^{dp} N_{d\sigma} N_{p\sigma'}. \quad (16)
\end{aligned}$$

This expression is strictly equal to:

$$\begin{aligned}
H_{int} = & \frac{1}{2} \sum_{\substack{(m,\sigma) \neq (m',\sigma') \\ m,m' \in \{d\}}} \tilde{U}_{m\sigma m'\sigma'}^{dd} n_{m\sigma} n_{m'\sigma'} \\
& + \frac{1}{2} \sum_{\substack{(m,\sigma) \neq (m',\sigma') \\ m,m' \in \{p\}}} \tilde{U}_{m\sigma m'\sigma'}^{pp} n_{m\sigma} n_{m'\sigma'} \\
& + U^{dp} \frac{N(N-1)}{2} \quad (17)
\end{aligned}$$

where $N = \sum_\sigma (N_{d\sigma} + N_{p\sigma})$ is the total number of electrons in p and d orbitals and $\tilde{U}^{dd} = U^{dd} - U^{dp}$, $\tilde{U}^{pp} = U^{pp} - U^{dp}$. In many compounds U^{pp} is of the order of U^{dp} , so that the \tilde{U}^{pp} term can be neglected. If, locally, the dominant screening mechanism is driven by the dp -interaction, one may consider the following assumption: adding charge onto the d -shell pushes away charge from the p -shell, such that the total charge on d - and p -shells is conserved. N is then a good quantum number, and the above rewriting corresponds to a reduction of a dp -Hamiltonian to an effective d - dp -one. We end up with a Hubbard model where only the d subspace is considered as correlated with a renormalized Coulomb interaction

$$\tilde{U}^{dd} = U^{dd} - U^{dp} \quad (18)$$

The same reasoning can be carried out in the presence of frequency-dependent interactions, and in Section V we will study the frequency-dependence of the resulting shell-folded interaction. In the following, we will discuss the shell-folded matrices, but simplify the notation such as to drop the tildes and superscripts. If nothing else is indicated, U will therefore mean the dd -part of the matrix.

Table I: Lattice parameters used for the iron pnictides and chalcogenides and energy windows \mathbb{W}_{dp} (in eV) for the d - dp low-energy Hamiltonians. d localized orbitals are constructed out of the Kohn-Sham states included in \mathbb{W}_{dp} .

	a(Å)	c(Å)	z_{As}	\mathbb{W}_{dp} (eV)
FeSe	3.77	5.50	0.267	[-6.5,2.4]
LiFeAs	3.79	6.36	0.2635	[-6.0,2.8]
BaFe ₂ As ₂	3.96	13.02	0.3545	[-6.5,2.7]
LaFeAsO	4.03	8.74	0.349	[-5.5,2.5]
BaRu ₂ As ₂	4.15	12.25	0.353	[-6.5,3.6]

III. HUBBARD INTERACTIONS AND SLATER PARAMETRIZATION IN PNICTIDES AND CHALCOGENIDES

A. General trends

We calculate the four-index-Coulomb interaction matrices $U_{m_1 m_2 m_3 m_4}$ from first-principles for a dp - dp Hamiltonian. Most matrix elements are of the order of 0.1 eV or less, except for two-index reduced interaction matrices, $U_{mm'}^{\sigma\sigma}|_{\text{cRPA}}$, $U_{mm'}^{\sigma\bar{\sigma}}|_{\text{cRPA}}$ and $J_{mm'}^{\text{cubic}}$ which can be extracted from the calculation. We then apply the shell-folding procedure described in Section II E. The values for the Hubbard U and Hund's exchange J for the effective d - dp low-energy Hamiltonian are reported in Table II. Here U is defined as the mean value of the full $U_{mm'}^{\sigma\bar{\sigma}}$ matrix while J is defined such that $U - J$ is the mean value of $U_{mm'}^{\sigma\sigma}$. For the latter matrix, the average is taken over the 20 non-diagonal (and thus non-zero) matrix elements. $4 \times 4 \times 3$, $5 \times 5 \times 2$, $4 \times 4 \times 2$ and $4 \times 4 \times 4$ meshes were used for the Brillouin zone integration for FeSe, LaFeAsO, LiFeAs and BaFe₂As₂ and BaRu₂As₂, respectively. The localized orbitals for Fe- $3d$ and Ru- $4d$ are constructed out of the Kohn-Sham states within the energy window \mathbb{W}_{dp} (Table I), within the implementation of Ref. [38].

FeSe is the material that exhibits the largest Hubbard $U = 3.9$ eV and Hund's exchange $J = 0.9$ eV. We obtain similar values within a direct calculation of a non-shell-folded d - dp model where only transitions from d to d bands are cut (see Ref. [49]), which was expected since there is negligible hybridization between Fe- d orbitals and Se- p orbitals. The values agree with the ones calculated within an implementation of cRPA employing maximally localized Wannier orbitals as Fe- $3d$ local orbitals^{42,46}. These relatively large (as compared to other pnictides) values for U and J have been used in LDA+DMFT calculations in Ref. 42: they lead to much more pronounced correlation effects than in iron pnictide compounds, in agreement with experiments^{56,57,76}. In particular, – in contrast to the iron pnictides – the calculations for FeSe found a lower energy feature that was identified as a lower Hubbard band⁴². This was confirmed by spectroscopic findings^{56,76}.

The Hubbard U within the d - dp low-energy Hamiltonian in the iron-based pnictides LaFeAsO and BaFe₂As₂ is about 1.5 eV smaller than in the chalcogenide FeSe

(see Table II). The screened ratios of the Slater integrals, F^4/F^2 , on the other hand, deviate more from the empirical atomic value for $3d$ shells.

In comparison, the values for the Hubbard U and Hund's coupling J for BaRu₂As₂ are lower than for BaFe₂As₂. Since the Ru- $4d$ orbitals are more extended than the Fe- $3d$ (as illustrated by the substantially larger bandwidth of the Ru- $4d$ bands, which is almost 2 eV larger than the one of Fe- $3d$), the kinetic energy of the Ru- $4d$ electrons is more important. As a consequence, correlations in BaRu₂As₂ are weak, and the DFT-LDA band structure without any further renormalisations is in good agreement with photoemission experiments⁷⁷.

Finally, LiFeAs can be considered as an intermediate case, where the Coulomb interactions are higher than in the two other materials. This trend can be linked to the longer Fe-As distance of 2.42 Å in this compound, compared to 2.40 Å in the others, resulting in more atomic-like iron Wannier functions.

B. Accuracy of the Slater parametrization

We now display the interaction matrices for FeSe, LiFeAs, BaFe₂As₂ and BaRu₂As₂ and discuss the accuracy of the Slater parametrization introduced in Section II C.

1. FeSe

Within the basis of cubic harmonics (using the ordering $d_{3z^2-r^2}, d_{x^2-y^2}, d_{xy}, d_{xz}, d_{yz}$) the effective local Hubbard interaction matrices (in eV) obtained starting from a cRPA calculation in a dp - dp model (see equations 4 and 5) and after shell-folding (see Eq. 18) with the intershell interaction $U_{dp} = 2.11$ eV read:

$$U_{mm'}^{\sigma\sigma}|_{\text{cRPA}} = \begin{pmatrix} 0 & 2.56 & 2.53 & 3.44 & 3.44 \\ 2.56 & 0 & 3.65 & 2.85 & 2.85 \\ 2.53 & 3.65 & 0 & 2.81 & 2.81 \\ 3.44 & 2.85 & 2.81 & 0 & 2.87 \\ 3.44 & 2.85 & 2.81 & 2.87 & 0 \end{pmatrix}$$

$$U_{mm'}^{\sigma\bar{\sigma}}|_{\text{cRPA}} = \begin{pmatrix} 4.97 & 3.36 & 3.33 & 3.95 & 3.95 \\ 3.36 & 4.94 & 4.06 & 3.55 & 3.55 \\ 3.33 & 4.06 & 4.85 & 3.52 & 3.52 \\ 3.95 & 3.55 & 3.52 & 4.99 & 3.56 \\ 3.95 & 3.55 & 3.52 & 3.56 & 4.99 \end{pmatrix}.$$

There is a small orbital dependence of the intra-orbital interactions, through the diagonal of $U_{mm'}^{\sigma\bar{\sigma}}|_{\text{cRPA}}$, since the cubic symmetry is an approximation for the crystal field in FeSe. The deviation is around 0.14 eV and the average intra-orbital interaction (before shell-folding) calculated with cubic symmetry is $U_m = 7.06$ eV.

Table II: Hubbard $U_{eff}(\equiv F^0 - U_{dp})$, Hund's exchange $J(\equiv (F^2 + F^4)/14)$ and screened ratio F^4/F^2 for effective (shell-folded) d - dp Hamiltonians. Both static ($\omega = 0$) and infinite frequency values are shown, as well as the unscreened (bare) interaction $v \equiv F^0(\omega = +\infty)$. The mean value of the intershell interaction $U_{dp}(0)$ and $U_{dp}(+\infty) = v_{dp}$ is also reported, along with the intrashell interaction $U_{pp}(0)$ and $U_{pp}(+\infty) = v_{pp}$. Values in parentheses (see also Ref. [46]) are indicated for comparison with cRPA calculations using maximally localized Wannier functions to represent the d local orbitals. We also show the value $U_{cut-d}(\omega = 0) \equiv F_{cut-d}^0(\omega = 0)$ of the interaction calculated in an “entangled” d - dp model where only $d \rightarrow d$ transitions are removed⁴⁹.

(eV)	U_{eff}	U_{cut-d}	J	F^4/F^2	U_{dp}	U_{pp}	$U_{eff}(+\infty)$	v	$J(+\infty)$	$F^4/F^2(+\infty)$	v_{dp}	v_{pp}
FeSe	3.90 (4.0 ⁴²)	3.97	0.92 (0.9 ⁴²)	0.699	2.11	4.02	14.32	20.36	1.03	0.623	6.04	10.18
LiFeAs	3.06	3.03	0.86	0.704	1.85	3.21	13.77	19.51	0.97	0.624	5.74	8.81
BaFe ₂ As ₂	2.30 (2.7 ⁵⁵)	2.53	0.81	0.725	1.33	2.42	13.73	19.31	0.96	0.620	5.58	8.39
LaFeAsO	1.97 (2.7 ³⁸)	2.43	0.77 (0.7 ³⁸)	0.732	1.17	2.10	13.23	18.74	0.92	0.622	5.51	8.20
BaRu ₂ As ₂	1.80	2.44	0.58	0.804	1.40	2.46	7.78	13.13	0.72	0.669	5.35	8.30

This deviation does not increase when elongating the crystal structure through the c -direction, perpendicular to the Fe-Se tetrahedra, although the dimensionality is reduced. This shows that the chemical environment of Fe is the main actor for the accuracy of the Slater parametrization.

For the Slater symmetrized reduced interaction matrices (in eV), we get from equations 10 and 11:

$$\bar{U}_{mm'}^{\sigma\sigma}|_{\text{Slater}} = \begin{pmatrix} 0 & 2.55 & 2.55 & 3.40 & 3.40 \\ 2.55 & 0 & 3.69 & 2.84 & 2.84 \\ 2.55 & 3.69 & 0 & 2.84 & 2.84 \\ 3.40 & 2.84 & 2.84 & 0 & 2.84 \\ 3.40 & 2.84 & 2.84 & 2.84 & 0 \end{pmatrix}$$

$$\bar{U}_{mm'}^{\sigma\bar{\sigma}}|_{\text{Slater}} = \begin{pmatrix} 4.95 & 3.35 & 3.35 & 3.92 & 3.92 \\ 3.35 & 4.95 & 4.11 & 3.54 & 3.54 \\ 3.35 & 4.11 & 4.95 & 3.54 & 3.54 \\ 3.92 & 3.54 & 3.54 & 4.95 & 3.54 \\ 3.92 & 3.54 & 3.54 & 3.54 & 4.95 \end{pmatrix}.$$

The deviation from the directly calculated values is of the order of 0.10 eV with a relative error of around 2%. Within the Slater parametrization the intra-orbital interactions are orbital-independent (that is, U_{mm} is independent of m).

Considering the higher-order Slater integrals, $F^2 = 7.57$ eV and $F^4 = 5.30$ eV, the screened ratio $F^4/F^2 = 0.70$ deviates from the empirical value of 0.63 (see Table II). Such deviation does not imply that the localized orbitals for Fe in FeSe display orbital anisotropies since the atomic parametrization appears to be well justified, as shown above. For the bare (unscreened) ratio $F^4/F^2|_{\text{bare}}$ we recover the atomic value.

2. LaFeAsO

For LaFeAsO, we find – again writing the matrix within the set of orbitals $d_{3z^2-r^2}, d_{x^2-y^2}, d_{xy}, d_{xz}, d_{yz}$ – and after shell-folding with the d -to-ligand interaction

$U_{dp} = 1.17$ eV:

$$U_{mm'}^{\sigma\sigma}|_{\text{cRPA}} = \begin{pmatrix} 0 & 0.94 & 0.85 & 1.53 & 1.53 \\ 0.94 & 0 & 1.82 & 1.12 & 1.12 \\ 0.85 & 1.82 & 0 & 1.00 & 1.00 \\ 1.53 & 1.12 & 1.00 & 0 & 1.00 \\ 1.53 & 1.12 & 1.00 & 1.00 & 0 \end{pmatrix}$$

$$U_{mm'}^{\sigma\bar{\sigma}}|_{\text{cRPA}} = \begin{pmatrix} 3.04 & 1.66 & 1.51 & 1.97 & 1.97 \\ 1.66 & 3.23 & 2.19 & 1.73 & 1.73 \\ 1.51 & 2.19 & 2.65 & 1.57 & 1.57 \\ 1.97 & 1.73 & 1.57 & 2.68 & 1.55 \\ 1.97 & 1.73 & 1.57 & 1.55 & 2.68 \end{pmatrix},$$

The intra-orbital repulsions are larger on the $d_{3z^2-r^2}$ and $d_{x^2-y^2}$ orbitals. This effect is due to the smaller orbital spreads of these orbitals that do not point toward the As ligands⁷⁸. The differences between the intra-orbital interactions for different orbitals are larger than in FeSe. In particular, the deviation yields 0.58 eV between the intra-orbital interactions on $d_{x^2-y^2}$ and d_{xy} orbitals, against 0.14 eV for FeSe.

Within the Slater parametrization, the symmetrized reduced interaction matrices read:

$$\bar{U}_{mm'}^{\sigma\sigma}|_{\text{Slater}} = \begin{pmatrix} 0 & 0.87 & 0.87 & 1.55 & 1.55 \\ 0.87 & 0 & 1.77 & 1.10 & 1.10 \\ 0.87 & 1.77 & 0 & 1.10 & 1.10 \\ 1.55 & 1.10 & 1.10 & 0 & 1.10 \\ 1.55 & 1.10 & 1.10 & 1.10 & 0 \end{pmatrix}$$

$$\bar{U}_{mm'}^{\sigma\bar{\sigma}}|_{\text{Slater}} = \begin{pmatrix} 2.85 & 1.53 & 1.53 & 1.98 & 1.98 \\ 1.53 & 2.85 & 2.13 & 1.68 & 1.68 \\ 1.53 & 2.13 & 2.85 & 1.68 & 1.68 \\ 1.98 & 1.68 & 1.68 & 2.85 & 1.68 \\ 1.98 & 1.68 & 1.68 & 1.68 & 2.85 \end{pmatrix}.$$

The largest discrepancy with the direct calculation, around 0.38 eV, is obtained for $d_{x^2-y^2}$. It is the hybridization with the As ligands and the covalent character of the As-Fe bonding that induce larger deviations from the atomic sphericity than in FeSe. Se atoms

have a Pauling electronegativity of around 2.55 that is larger than the one of As (2.18) or Fe (1.83). The more ionic character of the Fe-Se bonding makes the localized Fe-3d orbitals more atomic-like, and hence the Slater parametrization more accurate.

3. BaFe₂As₂ and BaRu₂As₂

Similar arguments can be employed for understanding the Slater parametrization for BaFe₂As₂. The interaction matrices (shell-folded with $U_{dp} = 1.33$ eV) now read

$$U_{mm'}^{\sigma\sigma}|_{\text{cRPA}} = \begin{pmatrix} 0 & 1.22 & 1.15 & 1.84 & 1.86 \\ 1.22 & 0 & 2.15 & 1.36 & 1.37 \\ 1.15 & 2.15 & 0 & 1.29 & 1.30 \\ 1.84 & 1.36 & 1.29 & 0 & 1.27 \\ 1.86 & 1.37 & 1.30 & 1.27 & 0 \end{pmatrix}$$

$$U_{mm'}^{\sigma\bar{\sigma}}|_{\text{cRPA}} = \begin{pmatrix} 3.47 & 1.96 & 1.86 & 2.31 & 2.33 \\ 1.96 & 3.47 & 2.53 & 1.99 & 2.00 \\ 1.86 & 2.53 & 3.11 & 1.89 & 1.90 \\ 2.31 & 1.99 & 1.89 & 3.04 & 1.85 \\ 2.33 & 2.00 & 1.90 & 1.85 & 3.07 \end{pmatrix}.$$

whereas the *Slater symmetrized* interaction matrices equal:

$$\bar{U}_{mm'}^{\sigma\sigma}|_{\text{Slater}} = \begin{pmatrix} 0 & 1.12 & 1.12 & 1.85 & 1.85 \\ 1.12 & 0 & 2.09 & 1.36 & 1.36 \\ 1.12 & 2.09 & 0 & 1.36 & 1.36 \\ 1.85 & 1.36 & 1.36 & 0 & 1.36 \\ 1.85 & 1.36 & 1.36 & 1.36 & 0 \end{pmatrix}$$

$$\bar{U}_{mm'}^{\sigma\bar{\sigma}}|_{\text{Slater}} = \begin{pmatrix} 3.22 & 1.82 & 1.82 & 2.30 & 2.30 \\ 1.82 & 3.22 & 2.47 & 1.98 & 1.98 \\ 1.82 & 2.47 & 3.22 & 1.98 & 1.98 \\ 2.30 & 1.98 & 1.98 & 3.22 & 1.98 \\ 2.30 & 1.98 & 1.98 & 1.98 & 3.22 \end{pmatrix}.$$

The largest discrepancy with the direct calculation is about 0.25 eV and is obtained for the $d_{3z^2-r^2}$ -orbital, which points toward the interlayer Ba planes and for $d_{x^2-y^2}$.

The larger hybridization of Ru 4d states with the As ligands also makes the atomic-like Slater parametrization less accurate. We note that the largest value of the screened ratio F^4/F^2 is obtained for this compound.

4. LiFeAs

The same procedure as above is applied to LiFeAs, where we find $U_{dp} = 1.85$ eV. Of all studied pnictides compounds, LiFeAs is the closest to FeSe with larger Coulomb interactions and lower screened ratio F^4/F^2 . We obtain for the interactions matrices after shell-folding:

$$U_{mm'}^{\sigma\sigma}|_{\text{cRPA}} = \begin{pmatrix} 0 & 1.84 & 1.82 & 2.64 & 2.64 \\ 1.84 & 0 & 2.84 & 2.05 & 2.05 \\ 1.82 & 2.84 & 0 & 2.02 & 2.03 \\ 2.64 & 2.05 & 2.02 & 0 & 2.05 \\ 2.64 & 2.05 & 2.03 & 2.05 & 0 \end{pmatrix}$$

$$U_{mm'}^{\sigma\bar{\sigma}}|_{\text{cRPA}} = \begin{pmatrix} 4.19 & 2.60 & 2.57 & 3.12 & 3.12 \\ 2.60 & 4.07 & 3.23 & 2.71 & 2.71 \\ 2.57 & 3.23 & 3.95 & 2.68 & 2.69 \\ 3.12 & 2.71 & 2.68 & 3.99 & 2.68 \\ 3.12 & 2.71 & 2.69 & 2.68 & 3.99 \end{pmatrix}.$$

whereas for the *Slater symmetrized* interaction matrices we obtain:

$$\bar{U}_{mm'}^{\sigma\sigma}|_{\text{Slater}} = \begin{pmatrix} 0 & 1.81 & 1.81 & 2.60 & 2.60 \\ 1.81 & 0 & 2.86 & 2.07 & 2.07 \\ 1.81 & 2.86 & 0 & 2.07 & 2.07 \\ 2.60 & 2.07 & 2.07 & 0 & 2.07 \\ 2.60 & 2.07 & 2.07 & 2.07 & 0 \end{pmatrix}$$

$$\bar{U}_{mm'}^{\sigma\bar{\sigma}}|_{\text{Slater}} = \begin{pmatrix} 4.04 & 2.55 & 2.55 & 3.08 & 3.08 \\ 2.55 & 4.04 & 3.25 & 2.73 & 2.73 \\ 2.55 & 3.25 & 4.04 & 2.73 & 2.73 \\ 3.08 & 2.73 & 2.73 & 4.04 & 2.73 \\ 3.08 & 2.73 & 2.73 & 2.73 & 4.04 \end{pmatrix}.$$

The parametrization is better than for other pnictides: the maximum discrepancy between the parametrized and the directly calculated matrices is only 0.15 eV. This, again, is the sign of more atomic-like Wannier functions, due to the larger Fe-As distance.

IV. SCREENING CHANNELS

In addition to the physically motivated Hubbard interactions – to be used in low-energy models for the respective compounds – other partially screened interactions can be constructed, with the aim of analyzing the importance of different screening processes. To this effect, we choose different particle-hole transitions (“screening channels”) that are removed from the RPA polarization. The effects of these screening channels are not additive, since the interaction depends on these different partial polarizations in a highly non-linear manner.

In this section, we calculate different partially screened interactions at zero frequency in the iron pnictides and chalcogenides and in SrVO₃. A detailed comparison allows us to understand global trends and to compare the relative importance of the screening contributions from the ligand p and from the d orbitals.

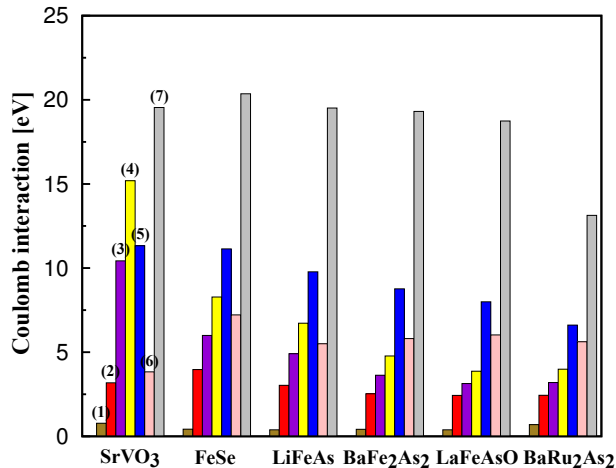


Figure 1: Strength of the screening channels in the comparison of an early transition metal oxide (SrVO₃) with iron-based pnictides. The bar charts show the static values of the monopole part of partially screened interactions for the 3d local orbitals within the dp low-energy Hamiltonians when removing specific “occupied to empty” transitions from the total RPA polarization. Cases (1) (brown) and (7) (gray) respectively correspond to the fully screened and unscreened cases. Case (2) (red) is the value of the static average intra-orbital interaction when removing $d \rightarrow d$ transitions only (corresponding to what is commonly denoted as d - dp Hamiltonian in the literature⁴⁵). Case (3) (purple) corresponds to the average intra-orbital interaction within the dp Hamiltonian, i.e. removing all the transitions within the energy window \mathbb{W}_{dp} , whereas in Case (4) (yellow), all the transitions involving p as well as $d \rightarrow d$ are removed. In Case (5) (blue), all the transitions involving d states are removed, whereas in Case (6) (salmon), only the transitions involving empty d states are considered.

A. Global trends along the pnictides and chalcogenide series

For each compound, we calculate seven different quantities at zero frequency, which are shown on Figure 1. The bare values on the local d orbitals vary less than 10% (except for the case of BaRu₂As₂ because of the larger extension of the 4d orbitals), as well as the fully screened values. Thus one can directly compare the values of the intra-orbital interactions obtained when considering specific occupied to empty transitions. While SrVO₃ stands out, the structure of the screening in all calculated pnictides and chalcogenide is remarkably similar.

If we look at the relative importance of the channels, one main difference between the different compounds is visible: the relative magnitude of the interaction in case (4) where all the transitions involving occupied p and all $d \rightarrow d$ transitions have been cut, and in case (6) where only the transitions from all occupied states (except d) to empty d states are considered. This is similar to comparing the screening of all occupied except p and d to all empty states except d (case (4)) with the screening of

$p \rightarrow d$ (case (6)). In FeSe where there is no interlayer atom and LiFeAs where Li electrons are deep core states, the number of channels of case (4) is reduced compared to the cases of BaFe₂As₂, LaFeAsO and BaRu₂As₂ where the interlayer atoms provide more screening channels. That is why the interaction in case (4) becomes bigger than in case (6) in FeSe and LiFeAs, while it is the opposite for other compounds.

For the same reason, the values of partially screened interactions are globally enhanced in FeSe and LiFeAs, because there are less possibilities of transitions. That is also why LaFeAsO displays lower values of the interaction. Eventually, the differences in screening within the pnictides and chalcogenides family happen to be mostly due to the interlayer structure.

B. Screening contributions from the ligands p orbitals

1. Ligand p to d transitions

To analyze these transitions we compare the values of cases (2) and (3) of Figure 1. The only difference between those two cases is precisely that ligand p to d transitions have been cut. In SrVO₃ the reduction of the Coulomb interaction due to this channel is remarkable, about 63%. Moreover, by comparing to the bare value and to the fully screened value, we see that these $d \rightarrow p$ transitions account for about 40% of the total screening. On the other hand, in pnictides and chalcogenides this reduction lies between 20% (LaFeAsO and BaRu₂As₂) and 33% (LiFeAs), two to three times less, and the $d \rightarrow p$ transitions account for only 10% of the total screening. This could be expected given the large number of ligands surrounding the metal in SrVO₃ and their ionic character. In the pnictides, the As-Fe electronegativity difference is smaller, thus the bonding is more covalent and the electrons are less free to rearrange their density to screen the charge. Moreover, if we think in terms of transitions from ligand filled to metal empty bands, there are simply more possibilities in SrVO₃ than in iron pnictides. Indeed, due to the low filling of the V-3d shell with only one electron, nearly all ligand to 3d transitions contribute to the screening in SrVO₃, while in the pnictides the d^6 filling prevents most such transitions.

2. Ligand p to other empty states

Now we compare cases (3) and (4). In case (4) all transitions from p states to other states than d have been further suppressed. Again we can see that while in SrVO₃ these transitions give a reduction of 29% of the Coulomb interaction, in the pnictides/chalcogenides it is only a reduction of 17% to 23%. The transitions from ligand p to other states are not as important as the transitions to

d states, which could be expected since the d states are closer to the Fermi level.

C. Screening contributions from d orbitals

Let us examine cases (5) and (6). In case (5) all transitions involving d states have been removed, while in case (6) only transitions to empty d states are considered. The difference can tell us how important the contribution of the d orbitals to the screening in the materials is.

1. SrVO_3

In SrVO_3 we see that the transitions to empty d states are nearly enough to recover the value obtained within a d - dp calculation. In this oxide the main channels are related to the empty d states, and the $p \rightarrow d$ channel is predominant. Still, suppressing all these channels allows to screen about 60% of the bare value.

2. *Pnictides and chalcogenides*

In the iron pnictides and chalcogenides the difference is not as impressive as in SrVO_3 . In the extreme case of BaRu_2As_2 , cases (5) and (6) nearly give the same result, showing that the empty d states are not as important. For $3d$ compounds, these transitions recover some predominance, and for FeSe and LiFeAs we can see that they account for a large part of the screening of the d - dp model. This importance is reduced in materials with interlayer screening atoms, as is also shown by the reduction of the value of case (5). Finally, we see that in pnictides and chalcogenides the main channels involve the d states. Also, this family is characterized by a very similar FeAs layer and the ligand p states are not dominant in the screening. This is why we attribute the small differences in the screening of the Coulomb interactions within the iron pnictides family to the interlayer structure. Indeed, the atoms between layers can participate to the screening by adding possibilities of transitions involving the d states, and the efficiency of these transitions depends on the material. We can also see this effect from an atomic point of view and presume that the higher polarizability of a large Ba ion in BaFe_2As_2 will be more efficient in screening the monopole interaction than the smaller Li ion in LiFeAs .

V. FREQUENCY DEPENDENCE

In this section, we discuss the frequency-dependence of the Hubbard interactions in the iron pnictides and chalcogenides and in SrVO_3 . We display the frequency-dependent intrashell and intershell interactions in the dp - dp Hamiltonian in which all transitions involving the

Fe- d and As- p orbitals are taken out. The structure of the high-frequency tail is compared to the free electron-like plasmon frequencies obtained for different numbers of electrons. We then calculate the strength of the bosonic renormalization factor and the impact of the shell-folding procedure on this quantity. Finally, we discuss the screening of the multipole Slater integrals.

A. High-frequency tail of the monopole interaction

We calculate the real part of the Slater integrals as a function of real frequency in the pnictides and chalcogenides. The same procedure is also applied to SrVO_3 to use this compound as a benchmark. A complete view of the dp - dp Hamiltonian before shell-folding is shown in Figure 2.

For non-entangled systems where the hybridization between the correlated atom and the ligand is small, the d bands can be clearly defined and separated from the ligand bands. As a consequence, calculating the strength of the static Coulomb interaction by shell folding of a dp - dp Hamiltonian or using a d - dp scheme where only transitions from and to bands with a majority of d -orbital character are cut and U_{dp} is neglected will give about the same result. That is the case in most iron pnictides because the entanglement is still relatively small and the d bands can be reasonably defined.

However, this is not true anymore if we look at the bare value. Indeed, the bare repulsion is essentially related to the spread of the Wannier function of the correlated orbital since no screening processes happen. So before shell-folding the strength of the Coulomb interaction within the d -shell is the same for both dp - dp and d - dp calculations. However there is a big difference in the treatment of the intershell interaction U_{dp} . While in a dp - dp model we see that the bare value of U_{dp} is much larger than the zero-frequency value, it is just ignored in a d - dp “entangled” calculation.

This motivates the application of frequency-dependent shell-folding. The results for all studied pnictides and chalcogenide are displayed on Figure 3, and compared to an “entangled” d - dp calculation where only transitions from and to bands with a majority of d -orbital character are cut.

For all compounds, at first sight the main correction introduced by the effective model is on the high-frequency tail, while the static part stays essentially the same. The infinite frequency value is lowered by about 30%. On the other hand, the frequency dependence of both models looks similar, with peaks around the same values of ω . Those peaks are less sharp in the effective model. Indeed F_0 and U_{dp} also share the same frequency dependence so $U_{eff} = F_0 - U_{dp}$ is smoothened compared to F_0 .

Interestingly, the case of SrVO_3 is much different from the pnictides, since both $U(0)$ and the high frequency tail are substantially modified when we take U_{dp} into consideration. Moreover, while in pnictides taking the p - d

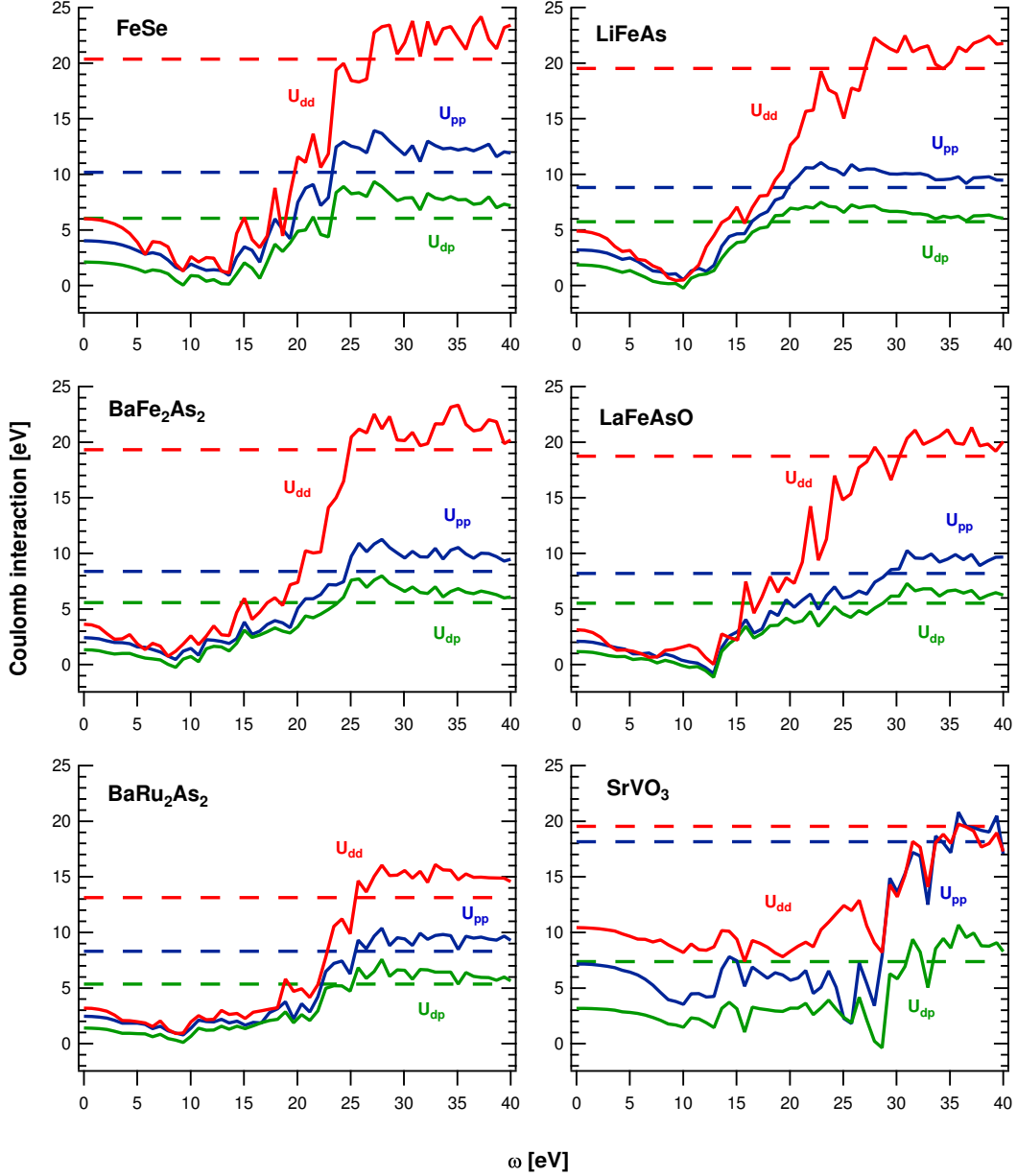


Figure 2: Frequency dependence of the different Hubbard interactions in the dp Hamiltonian without shell-folding. Here $U_{dd} = F^0$ and U_{pp} should be understood as the monopole part of the partially screened interactions. Dashed lines are the values at infinite frequency.

interactions into account leaves $U(0)$ stable or reduces it, in SrVO_3 $U(0)$ is increased. The correction of this value induced by the effective model seems to be in agreement with values used in many-body calculations where all d -orbitals are taken into account.

B. Plasmons and interband transitions

The dynamical structure of the Coulomb interaction is directly linked to the variations of the constrained polarization P^r . These variations are determined by inter-

band transitions and collective excitations. Indeed, in iron pnictides, ion-core polarization can be neglected, as shown by calculations of the constrained macroscopic dielectric function where all transitions from and to the valence electron bands have been cut. We calculate the energy of the main plasmon mode based on the free-electron formula for the plasma frequency:

$$\omega_p = \sqrt{\frac{ne^2}{m\epsilon_0}} \quad (19)$$

To calculate the density we take into account all va-

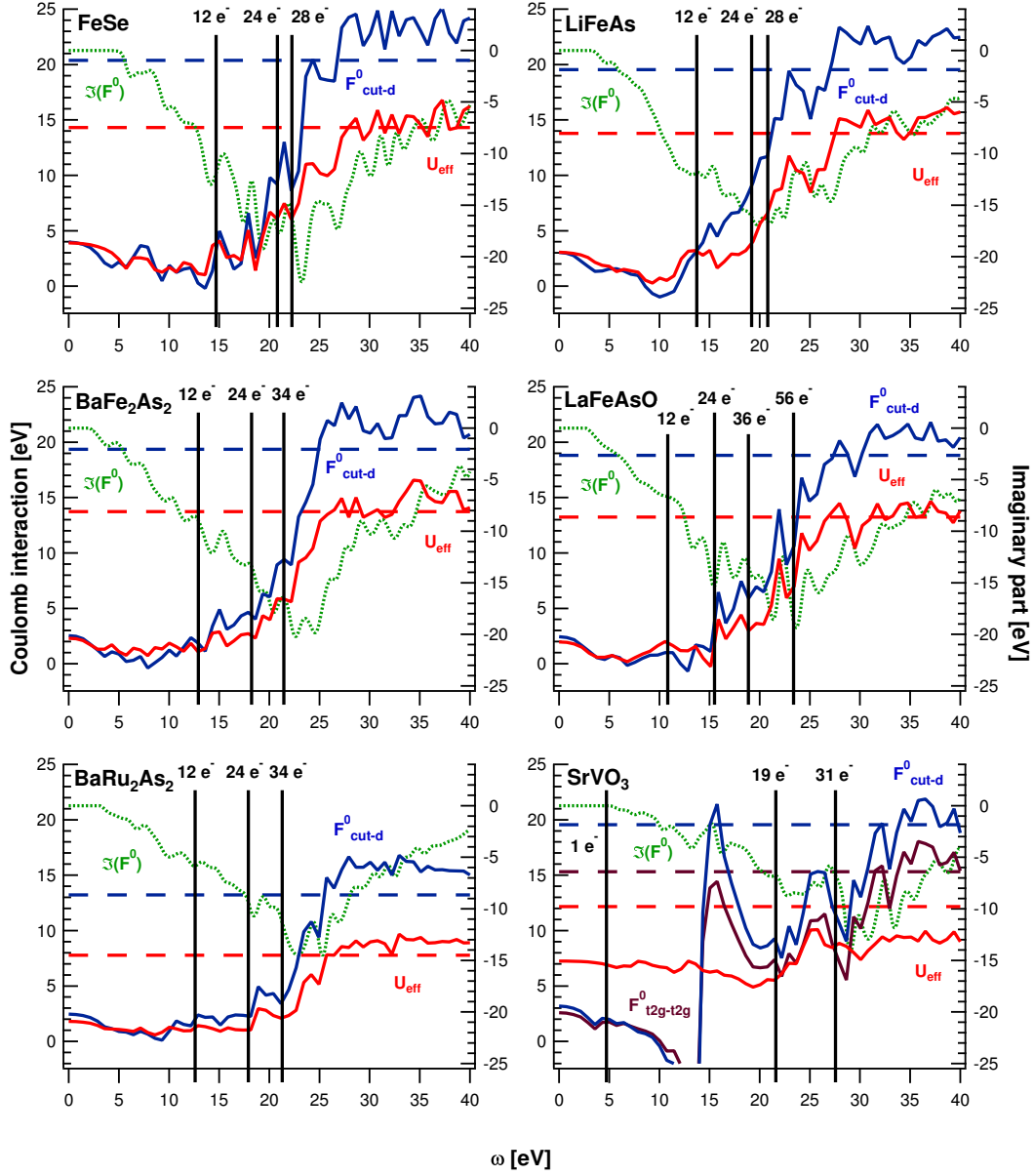


Figure 3: Frequency dependence of the monopole part of the partially screened Coulomb interaction within the d -shell. $U_{eff}(\omega)$ refers to $F^0(\omega) - U_{dp}(\omega)$ calculated in the dp - dp model. F^0_{cut-d} is the monopole part of the interaction calculated in an “entangled” d - dp model where only $d \rightarrow d$ transitions are removed. Dashed lines are the values at infinite frequency. The dotted line corresponds to the imaginary part of $F^0(\omega)$ and is compared to a free-electron calculation of the plasma frequency at partial resonances (vertical bars).

lence electrons, which corresponds to all bands down to -20 eV: the Fe 3d electrons, As or Se 4p and 4s electrons, Ba 4p in BaFe₂As₂ and BaRu₂As₂, and La 5p, O 2p and 2s in LaFeAsO. The binding energies of those electrons are still lower than the obtained plasma frequency (between 20 and 25 eV), so it is reasonable to think that they will enter the collective resonance. For SrVO₃ we take into account V 3d, O 2p, Sr 4p and O 2s electrons. The plasmon frequency is then compared to the imaginary part of the monopole interaction in a dp model (see the plasmon energy corresponding to the highest number

of electrons for each compound on Figure 3). We can see that the main peak of $\Im(F^0)$ agrees very well with the calculated plasmon frequency and corresponds to a cut-off frequency where the Coulomb interaction increases sharply from the static value to the infinite frequency value.

We also show that some of the other peaks could be assigned to partial plasmon resonances. The first partial resonance would correspond to the number of Fe 3d (or V 3d) electrons. For the second one, we add the As or Se 4p electrons (or the O 2p in the case of SrVO₃). We

also show a third partial resonance in LaFeAsO, corresponding to the addition of the O $2p$ electrons. However, it is difficult to make a one-to-one correspondence because of the entanglement of the plasmons with the interband transitions which creates rather a continuum of screening modes. This effect has been documented in transition metals, where the interband transitions from the d bands to higher bands act to shift and broaden the plasmons composed of s and p electrons⁷⁹. It also happens in the pnictides and chalcogenides since there are possibilities of transitions at frequencies close to the one of the free-electron plasmon. As an illustration, we can see in the case of SrVO₃ that the agreement between a partial resonance of O $2p$ and V $3d$ electrons with the plasmon around 15 eV is really bad. However, the free-electron plasma frequency of about 21.5 eV is likely to be modified by a combination of possible interband transitions in this frequency range and background polarization provided by lower-lying states. Indeed, the calculation of the constrained macroscopic dielectric function where transitions from dp bands to all empty states have been removed gives a value of about 1.4 at $\omega = 16$ eV. Simply taking this background macroscopic dielectric function into account would already reduce the plasma frequency to around 18 eV. Further adding the contribution of the possible interband transitions could easily shift the value of the plasma frequency to 15 eV.

C. Density of screening modes

We can now examine the impact of taking into account the d - p interaction on $\Im(U(\omega))/\omega^2$, which can be physically understood as the density of screening modes and determines Z_B (see Figure 4). Though the global structure is conserved, a strong renormalization is induced.

Two effects are successively involved. First, we cut more transitions in the cRPA calculation in the dp - dp model. This will have an impact at low frequency, especially if the first transitions happening in the d - dp model were from occupied p to empty d . In that case the gap of the screening modes, that is to say the energy needed for the first transition between occupied and empty bands, will increase. At higher frequencies, the difference is largely negligible. Indeed, most of the screening processes do not involve $p \rightarrow d$ transitions, as shown in Section IV. The second effect is due to the shell-folding procedure. Due to the fact that U_{dd} and U_{dp} share variations in frequency, the frequency dependence of the effective interaction is flattened. Eventually, most of the dynamical structure of the screening stays unchanged when we suppress $p \rightarrow d$ transitions, and the main effect of shell-folding is a reduction of the density of screening modes.

One could wonder about the validity of the different models depending on the frequency. At very low frequency (below the gap of the d - dp model), the d - dp model result is adapted for the pnictides, because the entanglement is not too strong and the bands can be relatively

well separated. However, as soon as the frequency becomes larger than the gap, this low-energy model is not valid anymore in the sense of the renormalization group. For higher frequencies, this is all the more true since the Coulomb interaction between d and p orbitals is even higher and cannot be neglected.

D. Bosonic renormalization factor Z_B

We focus on the impact of the shell-folding procedure on the bosonic renormalization factor Z_B introduced in Section IID. The smaller density of screening modes in the effective model lowers the value of Z_B since

$$\ln(Z_B) = - \int_0^{+\infty} \frac{\Im U_{ret}(\omega)}{\pi \omega^2} d\omega \quad (20)$$

We compare the values obtained for a d - dp model with and without shell-folding in Table III.

At low frequency, the spectral weight reduction of the quasiparticles is $Z_{eff} \times Z_B$ where Z_{eff} is the renormalization obtained in a static Hubbard model⁴⁷. Z_{eff} depends on $U(0)/D$ with D the bandwidth. In the pnictides case, $U(0)$ is nearly the same in the two calculations. Qualitatively, Z_{eff} will be a little bigger in the effective model since both $U(0)$ is slightly smaller and the bandwidth is larger due to a higher Z_B . So the discrepancies between the two models as to the physical properties of the system will be largely dependent on the bosonic renormalization factor Z_B . Eventually, the renormalization is substantially changed when we take into account the p - d interactions.

As for SrVO₃, the bosonic renormalization factor Z_B in the effective model is equal to 0.93, which should be compared to a value of 0.70 in a t_{2g} - t_{2g} model (0.64 when cutting only the transitions from and to the d -like bands). We see that in this compound U_{eff} is very close to being static, while in the pnictides there is still a large frequency dependence even in the effective model. Indeed, U_{eff} is less screened in SrVO₃: the infinite frequency value is reduced by 40%, while in the pnictides the reduction is much higher, from 70% in FeSe to 85% in LaFeAsO. This indicates a low coupling to the plasmon. The reason is that the main plasmon around 15 eV in SrVO₃ is due to transitions from occupied O- p to empty V- eg states (see Figures 4 and 1), which are suppressed in a dp - dp model. The shell-folding procedure allows us to take into account the intershell p - d interaction that was ignored in an entangled d - dp model. However, when we project our dp - dp model into an effective d - dp model we lose the possibility to reintroduce the screening from $p \rightarrow d$ transitions – which might also necessitate a more refined model including long-range interactions. We mention in particular that the frequency-dependence of the effective local interaction is expected to become stronger when non-local screening processes within the low-energy manifold are taken into account. This would correspond to a generalisation of what has been worked

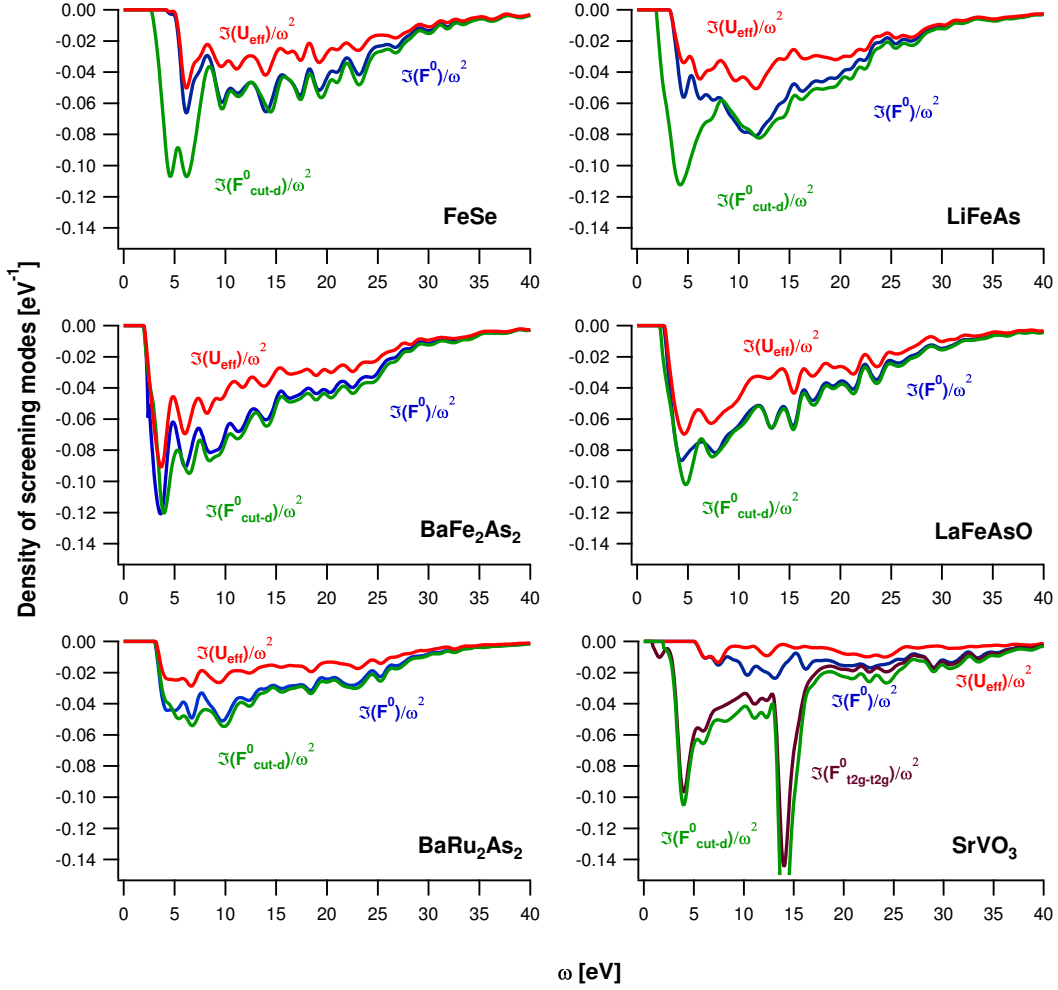


Figure 4: Density of screening modes in iron pnictides and chalcogenides before and after shell folding of a dp - dp model compared to an entangled d - dp model. SrVO_3 is also shown for comparison.

Table III: Values of Z_B extracted from the monopole part of the interaction within the d -shell. Results for the shell-folded dp - dp model and for the directly calculated d - dp model are displayed.

	FeSe	LiFeAs	BaFe ₂ As ₂	LaFeAsO	BaRu ₂ As ₂
Z_B (effective)	0.78	0.76	0.71	0.73	0.85
Z_B (entangled)	0.63	0.60	0.59	0.62	0.74

out in⁸⁰ for the static part of the effective interactions. These arguments demonstrate that the choice of the appropriate low-energy Hamiltonian remains a subtle and crucial question, since the effects contained within the different models are not the same.

E. Dynamical J

We will now focus on the Hund's coupling matrix

$$J_{mm'} = U_{mm'm'm, m \neq m'} \quad (21)$$

In a cubic basis we can define:

$$\bar{J} \equiv \frac{5}{7} \frac{F^2 + F^4}{14} \quad (22)$$

which physically corresponds to an arithmetic mean of all elements $J_{mm'}$. This quantity is frequency-dependent and differs by a factor $5/7$ from the definition of Section II C – which is more adapted to the case of a model defined only by U and J , while here we are considering the full orbital-dependent matrix. In BaFe_2As_2 , it will vary by about 17%, from 0.58 eV at zero frequency to 0.68 eV at infinite frequency. However, if one looks at the full J

matrix at zero frequency, we find:

$$J_{mm'}|_{\text{cRPA}} = \begin{pmatrix} 0 & 0.74 & 0.71 & 0.47 & 0.47 \\ 0.74 & 0 & 0.38 & 0.63 & 0.63 \\ 0.71 & 0.38 & 0 & 0.60 & 0.60 \\ 0.47 & 0.63 & 0.60 & 0 & 0.58 \\ 0.47 & 0.63 & 0.60 & 0.58 & 0 \end{pmatrix}.$$

where the order of the orbitals is, as before, $d_{3z^2-r^2}, d_{x^2-y^2}, d_{xy}, d_{xz}, d_{yz}$.

We also give the corresponding bare J

$$J_{mm'}|_{\text{cRPA}} = \begin{pmatrix} 0.0 & 0.88 & 0.86 & 0.52 & 0.52 \\ 0.88 & 0.0 & 0.40 & 0.74 & 0.74 \\ 0.86 & 0.40 & 0.0 & 0.73 & 0.73 \\ 0.52 & 0.74 & 0.73 & 0.0 & 0.71 \\ 0.52 & 0.74 & 0.73 & 0.71 & 0.0 \end{pmatrix}$$

and the Slater-parametrized version of the low-frequency J :

$$J_{mm'}|_{\text{cRPA}} = \begin{pmatrix} 0.0 & 0.70 & 0.70 & 0.45 & 0.45 \\ 0.70 & 0.0 & 0.38 & 0.62 & 0.62 \\ 0.70 & 0.38 & 0.0 & 0.62 & 0.62 \\ 0.45 & 0.62 & 0.62 & 0.0 & 0.62 \\ 0.45 & 0.62 & 0.62 & 0.62 & 0.0 \end{pmatrix}$$

The spread of the elements of these matrices is really large: for instance, the $d_{z^2} \longleftrightarrow d_{x^2-y^2}$ element is about twice the $d_{x^2-y^2} \longleftrightarrow d_{xy}$ element, in all three matrices, demonstrating that this is a consequence of the different orbital extensions. Consequently, J is not a good quantity to focus on, and it is better to look at the frequency-dependence of the Slater integrals F^2 and F^4 . This is shown on Figure 5. While F^4 shows very little variation with ω , F^2 exhibits a minimum at an intermediate frequency which corresponds to the onset of interband transitions. It is also a minimum of J and a maximum of F^4/F^2 .

In a DMFT calculation, one can wonder how to deal with this non-monopole frequency dependence. We suggest several answers. Using the bare value for F^2 and F^4 is satisfying from a model point of view. At infinite frequency the Slater parametrization of the Coulomb interaction matrix is excellent because the system is atomic like. Then one can assume that the plasmon is only screening the monopole part of the interaction. On the other hand, the low-energy properties of the system are more influenced by the static part of the interaction. In this view, the best would be to parametrize the Coulomb interaction matrix at low frequency as well as possible, and then to ignore again the effects of the plasmons on the non-monopole terms. Finally, one could also consider a fully frequency-dependent matrix, using for example the double expansion algorithm of Steiner et al.⁸¹.

VI. CONCLUSION

In conclusion, we have studied the strength of the effective Hubbard interactions and the accuracy of the Slater parametrization in the iron pnictides for a shell-folded dp - dp model. In agreement to what was found in Ref. 49 for the d - dp model, we find that the effective Coulomb interactions for Fe- $3d$ shells are larger in 11 than in 122 and 1111 pnictides, while the 111 pnictides are an intermediate case, and that the accuracy of the Slater parametrization depends on the ligand-metal bonding character rather than on the dimensionality of the lattice: it is excellent for ionic-like FeSe and not as good for more covalent Fe-As (LaFeAsO, BaFe₂As₂) pnictides. The main effect of the shell-folding procedure is to reduce the value of the high-frequency value of the Coulomb interaction by about 30%.

We have discussed the relative importance of screening channels which reduce the on-site bare interaction to the fully screened one. We have shown that the screening channels are analogously structured in the pnictides and chalcogenides family, while this structure is very different in the benchmark oxide SrVO₃. The ligand channel does not appear to be responsible for the dominant screening mechanism in iron pnictides.

We have calculated the full frequency dependence of the Hubbard interaction in the 11, 111, 122 and 1111 families of iron pnictides and compared it to SrVO₃ in the dp - dp model, including both Fe- d and As- p degrees of freedom. We have calculated the free-electron plasma frequencies corresponding to different numbers of electrons involved in the resonance, and we have shown that the screening modes could not be approximated by a single plasmon as in SrVO₃.

Finally, we have studied the effect of the shell-folding procedure and compared the so-constructed effective d - dp model to a d - dp model where only transitions from and to bands with a majority of d -orbital character are cut and U_{dp} is neglected. We find an important reduction of the high-frequency tail which results in a less important bosonic renormalization factor Z_B (that is, closer to one).

ACKNOWLEDGMENTS

We acknowledge useful discussions with M. Aichhorn, F. Aryasetiawan, M. Casula, A. Georges, C. Martins, T. Miyake and G. Sawatzky. This work was supported by the European Research Council under its Consolidator grant scheme (project number 617196), IDRIS/GENCI under project t2016091393, the Natural Science Foundation of China (Projects No. 21211130098, 21373017 and 21321001) and the Cai Yuanpei program.

* Electronic address:
ambroise.van-roekeghem@polytechnique.edu

¹ P. J. Hirschfeld, Comptes Rendus Physique **17**, 197

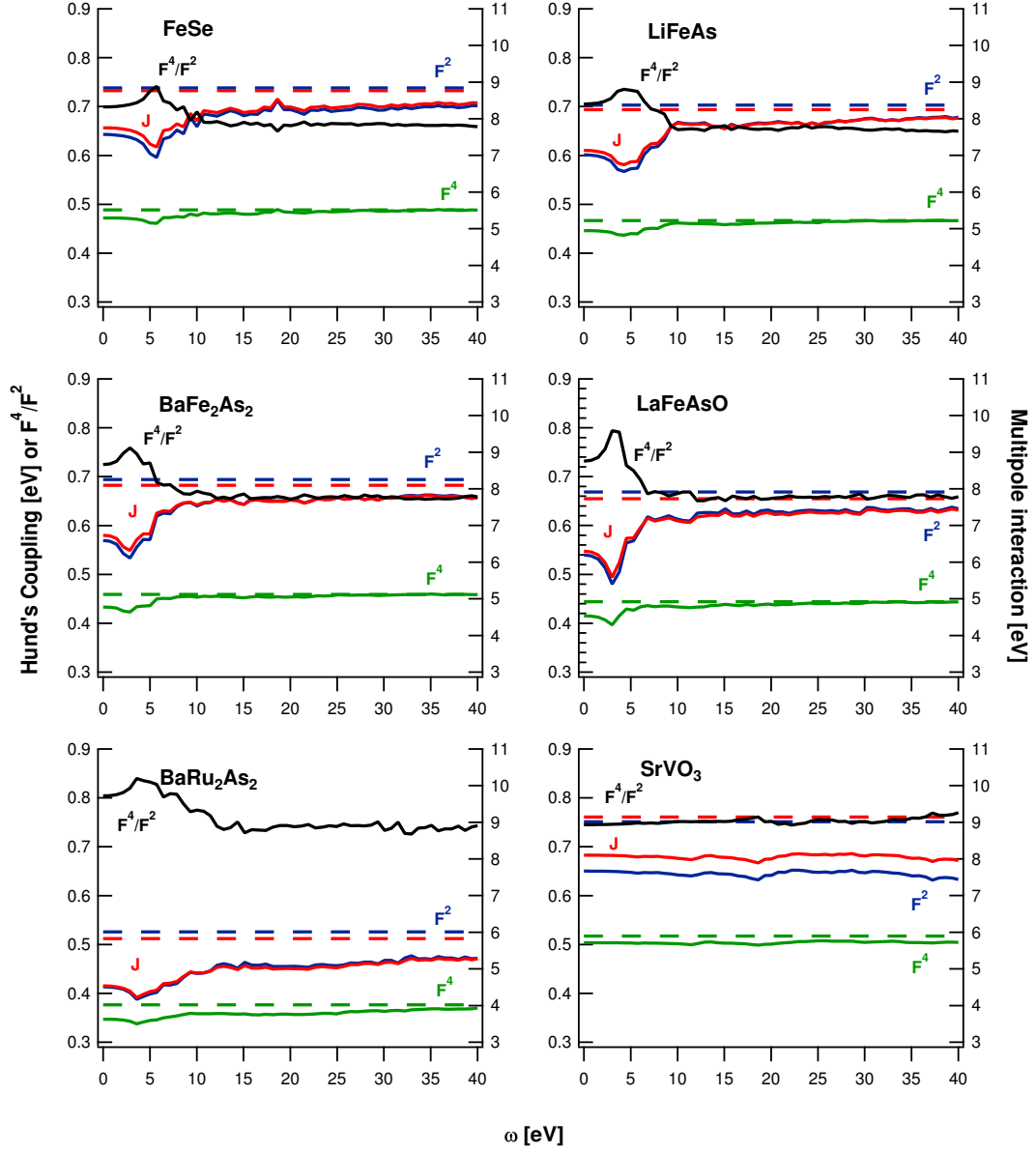


Figure 5: Frequency dependence of F^2 , F^4 and $\bar{J} \left(\equiv \frac{5}{7} \frac{F^2 + F^4}{14} \right)$ calculated in a dp - dp model. Dashed lines are the values at infinite frequency. Note the different energy scales for the Slater integrals (right scale) and for \bar{J} (left scale), in eV. Also shown is the unitless ratio F^4/F^2 , using the left scale, but of course in this case as a dimensionless scale.

(2016), ISSN 1631-0705, iron-based superconductors / Supraconducteurs à base de fer.

² F. Rullier-Albenque, Comptes Rendus Physique **17**, 164 (2016), ISSN 1631-0705, iron-based superconductors / Supraconducteurs à base de fer.

³ A. van Roekeghem, P. Richard, H. Ding, and S. Biermann, Comptes Rendus Physique **17**, 140 (2016), ISSN 1631-0705, iron-based superconductors / Supraconducteurs à base de fer.

⁴ Y. Kamihara, T. Watanabe, M. Hirano, and H. Hosono, J. Am. Chem. Soc. **130**, 3296 (2008).

⁵ Z.-A. Ren, L. Wei, Y. Jie, Y. Wei, S. Xiao-Li, Zheng-Cai, C. Guang-Can, D. Xiao-Li, S. Li-Ling, Z. Fang, et al., Chin. Phys. Lett. **25**, 2215 (2008).

⁶ G. F. Chen, Z. Li, D. Wu, G. Li, W. Z. Hu, J. Dong, P. Zheng, J. L. Luo, and N. L. Wang, Phys. Rev. Lett. **100**, 247002 (2008).

⁷ H.-H. Wen, G. Mu, L. Fang, H. Yang, and X. Zhu, Eur. Phys. Lett. **82**, 17009 (2008).

⁸ X. H. Chen, T. Wu, G. Wu, R. H. Liu, H. Chen, and D. F. Fang, Nature **453**, 761 (2008).

⁹ M. Rotter, M. Tegel, and D. Johrendt, Phys. Rev. Lett. **101**, 107006 (2008).

¹⁰ A. S. Sefat, R. Jin, M. A. McGuire, B. C. Sales, D. J. Singh, and D. Mandrus, Phys. Rev. Lett. **101**, 117004 (2008).

¹¹ S. Sharma, A. Bharathi, S. Chandra, V. R. Reddy, S. Paulraj, A. T. Satya, V. S. Sastry, A. Gupta, and C. S. Sundar, Phys. Rev. B **81**, 174512 (2010).

- ¹² J. H. Tapp, Z. Tang, B. Lv, K. Sasmal, B. Lorenz, P. C. W. Chu, and A. M. Guloy, *Phys. Rev. B* **78**, 060505 (2008).
- ¹³ X. Wang, Q. Liu, Y. Lv, W. Gao, L. Yang, R. Yu, F. Li, and C. Jin, *Solid State Commun.* **148**, 538 (2008).
- ¹⁴ M. J. Pitcher, D. R. Parker, P. Adamson, S. J. Herkelrath, A. T. Boothroyd, R. M. Ibberson, M. Brunelli, and S. J. Clarke, *Chem. Commun.* pp. 5918–5920 (2008).
- ¹⁵ F.-C. Hsu, J.-Y. Luo, K.-W. Yeh, T.-K. Chen, T.-W. Huang, P. M. Wu, Y.-C. Lee, Y.-L. Huang, Y.-Y. Chu, D.-C. Yan, et al., *Proc. Natl. Acad. Sci. U.S.A.* **105**, 14262 (2008).
- ¹⁶ S. Margadonna, Y. Takabayashi, Y. Ohishi, Y. Mizuguchi, Y. Takano, T. Kagayama, T. Nakagawa, M. Takata, and K. Prassides, *Phys. Rev. B* **80**, 064506 (2009).
- ¹⁷ K.-W. Yeh, T.-W. Huang, Y.-l. Huang, T.-K. Chen, F. Hsu, P. M. Wu, Y. C. Lee, Y.-Y. Chu, C.-L. Chen, J.-Y. Luo, et al., *Eur. Phys. Lett.* **84**, 37002 (2008).
- ¹⁸ L. de’ Medici, G. Giovannetti, and M. Capone, *Phys. Rev. Lett.* **112**, 177001 (2014).
- ¹⁹ T. Misawa, K. Nakamura, and M. Imada, *Phys. Rev. Lett.* **108**, 177007 (2012).
- ²⁰ A. N. Yaresko, G.-Q. Liu, V. N. Antonov, and O. K. Andersen, *Phys. Rev. B* **79**, 144421 (2009).
- ²¹ I. I. Mazin, M. D. Johannes, L. Boeri, K. Koepernik, and D. J. Singh, *Phys. Rev. B* **78**, 085104 (2008).
- ²² A. Subedi, L. Zhang, D. J. Singh, and M. H. Du, *Phys. Rev. B* **78**, 134514 (2008).
- ²³ K. Ishida, Y. Nakai, and H. Hosono, *J. Phys. Soc. Jpn.* **78**, 062001 (2009).
- ²⁴ N. Qureshi, Y. Drees, J. Werner, S. Wurmehl, C. Hess, R. Klingeler, B. Büchner, M. T. Fernandez-Diaz, and M. Braden, *Phys. Rev. B* **82**, 184521 (2010).
- ²⁵ G. A. Sawatzky, I. S. Elfimov, J. van den Brink, and J. Zanen, *Eur. Phys. Lett.* **86**, 17006 (2009).
- ²⁶ Q. Huang, Y. Qiu, W. Bao, M. A. Green, J. W. Lynn, Y. C. Gasparovic, T. Wu, G. Wu, and X. H. Chen, *Phys. Rev. Lett.* **101**, 257003 (2008).
- ²⁷ S. Li, C. de la Cruz, Q. Huang, Y. Chen, J. W. Lynn, J. Hu, Y.-L. Huang, F.-C. Hsu, K.-W. Yeh, M.-K. Wu, et al., *Phys. Rev. B* **79**, 054503 (2009).
- ²⁸ P. Hansmann, R. Arita, A. Toschi, S. Sakai, G. Sangiovanni, and K. Held, *Phys. Rev. Lett.* **104**, 197002 (2010).
- ²⁹ A. Toschi, R. Arita, P. Hansmann, G. Sangiovanni, and K. Held, *Phys. Rev. B* **86**, 064411 (2012).
- ³⁰ P. Hansmann, T. Ayrar, A. Tejada, and S. Biermann, *arXiv: 1511.05004* (2015).
- ³¹ A. Georges, G. Kotliar, W. Krauth, and M. J. Rozenberg, *Rev. Mod. Phys.* **68**, 13 (1996).
- ³² G. Kotliar, S. Y. Savrasov, K. Haule, V. S. Oudovenko, O. Parcollet, and C. A. Marianetti, *Rev. Mod. Phys.* **78**, 865 (2006).
- ³³ V. I. Anisimov, A. Poteryaev, M. Korotin, A. Anokhin, and G. Kotliar, *J. Phys.: Condens. Matter* **9**, 943 (1997).
- ³⁴ A. I. Lichtenstein and M. I. Katsnelson, *Phys. Rev. B* **57**, 6884 (1998).
- ³⁵ V. I. Anisimov, D. Korotin, M. Korotin, A. V. Kozhevnikov, J. Kunes, S. A. O., S. L. Skornyakov, and S. V. Streltsov, *J. Phys. Condens. Matter* **21**, 075602 (2009).
- ³⁶ A. O. Shorikov, M. A. Korotin, S. V. Streltsov, S. L. Skornyakov, D. M. Korotin, and V. I. Anisimov, *J. Exp. Theor. Phys.* **108**, 121 (2009).
- ³⁷ V. I. Anisimov, D. M. Korotin, S. V. Streltsov, A. V. Kozhevnikov, J. Kunes, S. A. O., and M. A. Korotin, *JETP Lett.* **88**, 729 (2008).
- ³⁸ M. Aichhorn, L. Pourovskii, V. Vildosola, M. Ferrero, O. Parcollet, T. Miyake, A. Georges, and S. Biermann, *Phys. Rev. B* **80**, 085101 (2009).
- ³⁹ K. Haule, J. H. Shim, and G. Kotliar, *Phys. Rev. Lett.* **100**, 226402 (2008).
- ⁴⁰ K. Haule and G. Kotliar, *New J. Phys.* **11**, 025021 (2009).
- ⁴¹ A. Liebsch and H. Ishida, *Phys. Rev. B* **82**, 155106 (2010).
- ⁴² M. Aichhorn, S. Biermann, T. Miyake, A. Georges, and M. Imada, *Phys. Rev. B* **82**, 064504 (2010).
- ⁴³ K. Haule, C.-H. Yee, and K. Kim, *Phys. Rev. B* **81**, 195107 (2010).
- ⁴⁴ F. Aryasetiawan, M. Imada, A. Georges, G. Kotliar, S. Biermann, and A. I. Lichtenstein, *Phys. Rev. B* **70**, 195104 (2004).
- ⁴⁵ T. Miyake, L. Pourovskii, V. Vildosola, S. Biermann, and A. Georges, *J. Phys. Soc. Jpn. : Supplement C* **77**, 99 (2008).
- ⁴⁶ T. Miyake, K. Nakamura, R. Arita, and M. Imada, *J. Phys. Soc. Jpn.* **79**, 044705 (2010).
- ⁴⁷ M. Casula, P. Werner, L. Vaugier, F. Aryasetiawan, T. Miyake, A. J. Millis, and S. Biermann, *Phys. Rev. Lett.* **109**, 126408 (2012).
- ⁴⁸ K. Nakamura, R. Arita, and M. Imada, *J. Phys. Soc. Jpn.* **77**, 093711 (2008).
- ⁴⁹ L. Vaugier, Ph.D. thesis, Ecole Polytechnique, France (2011).
- ⁵⁰ J.-Z. Ma, A. van Roekeghem, P. Richard, Z.-H. Liu, H. Miao, L.-K. Zeng, N. Xu, M. Shi, C. Cao, J.-B. He, et al., *Phys. Rev. Lett.* **113**, 266407 (2014).
- ⁵¹ A. van Roekeghem, T. Ayrar, J. M. Tomczak, M. Casula, N. Xu, H. Ding, M. Ferrero, O. Parcollet, H. Jiang, and S. Biermann, *Phys. Rev. Lett.* **113**, 266403 (2014).
- ⁵² A. van Roekeghem, P. Richard, X. Shi, S.-F. Wu, L.-K. Zeng, B. I. Saparov, Y. Ohtsubo, T. Qian, A. Safa-Sefat, S. Biermann, et al., *arXiv:1505.00753* (2015).
- ⁵³ N. Xu, P. Richard, A. van Roekeghem, P. Zhang, H. Miao, W.-L. Zhang, T. Qian, M. Ferrero, A. S. Sefat, S. Biermann, et al., *Phys. Rev. X* **3**, 011006 (2013).
- ⁵⁴ E. Razzoli, C. E. Matt, M. Kobayashi, X.-P. Wang, V. N. Strocov, A. van Roekeghem, S. Biermann, N. C. Plumb, M. Radovic, T. Schmitt, et al., *Phys. Rev. B* **91**, 214502 (2015).
- ⁵⁵ P. Werner, M. Casula, T. Miyake, F. Aryasetiawan, A. J. Millis, and S. Biermann, *Nature Physics* **8**, 331 (2012).
- ⁵⁶ R. Yoshida, T. Wakita, H. Okazaki, Y. Mizuguchi, S. Tsuda, Y. Takano, H. Takeya, K. Hirata, T. Muro, M. Okawa, et al., *J. Phys. Soc. Jpn.* **78**, 034708 (2009).
- ⁵⁷ A. Tamai, A. Y. Ganin, E. Rozbicki, J. Bacsá, W. Meevasana, P. D. C. King, M. Caffio, R. Schaub, S. Margadonna, K. Prassides, et al., *Phys. Rev. Lett.* **104**, 097002 (2010).
- ⁵⁸ S. Biermann, *J. Phys. Condens. Matter* **26**, 173202 (2014).
- ⁵⁹ M. Casula, A. Rubtsov, and S. Biermann, *Phys. Rev. B* **85**, 035115 (2012).
- ⁶⁰ A. van Roekeghem and S. Biermann, *EPL* **108**, 75003 (2014).
- ⁶¹ S. Biermann and A. van Roekeghem, *arXiv:1512.08499*, *J. El. Sp.* (2015).
- ⁶² L. Vaugier, H. Jiang, and S. Biermann, *Phys. Rev. B* **86**, 165105 (2012).
- ⁶³ P. Blaha, K. Schwarz, G. Madsen, D. Kvasnicka, and J. Luitz, *Wien2k, An Augmented Plane Wave+Local Orbitals Program for Calculating Crystal Properties* (Tech.

- Universität Wien, Austria, 2001).
- ⁶⁴ P. Seth, P. Hansmann, A. van Roekeghem, L. Vaugier, and S. Biermann, arXiv:1508.07466 (2015).
- ⁶⁵ B. R. Judd, *Operator Techniques in Atomic Spectroscopy* (Princeton University Press, 1998).
- ⁶⁶ J. C. Slater, *Quantum Theory of Atomic Structure*, vol. 1 (McGraw-Hill, New York, 1960).
- ⁶⁷ S. Sugano, Y. Tanabe, and H. Kamimura, *Multiplets of transition-metal ions in crystal*, vol. 1 (Academic Press, New York London, 1970).
- ⁶⁸ V. I. Anisimov, F. Aryasetiawan, and A. I. Lichtenstein, J. Phys.: Condens. Matter **9**, 767 (1997).
- ⁶⁹ A. Kutepov, K. Haule, S. Y. Savrasov, and G. Kotliar, Phys. Rev. B **82**, 045105 (2010).
- ⁷⁰ E. Antonides, E. C. Janse, and G. A. Sawatzky, Phys. Rev. B **15**, 1669 (1977).
- ⁷¹ G. A. Sawatzky and J. W. Allen, Phys. Rev. Lett. **53**, 2339 (1984).
- ⁷² D. van der Marel, G. A. Sawatzky, and F. U. Hillebrecht, Phys. Rev. Lett. **53**, 206 (1984).
- ⁷³ I. J. Lang and Y. A. Firsov, Sov. Phys. JETP **16**, 1301 (1962).
- ⁷⁴ P. Werner and A. Millis, Phys. Rev. Lett. **99**, 146404 (2007).
- ⁷⁵ C. Herring, *Magnetism: Exchange interactions among itinerant electrons*, vol. 4 (Academic Press, 1966).
- ⁷⁶ A. Yamasaki, Y. Matsui, S. Imada, K. Takase, H. Azuma, T. Muro, Y. Kato, A. Higashiya, A. Sekiyama, S. Suga, et al., Phys. Rev. B **82**, 184511 (2010).
- ⁷⁷ V. Brouet, F. Rullier-Albenque, M. Marsi, B. Mansart, M. Aichhorn, S. Biermann, J. Faure, L. Perfetti, A. Taleb-Ibrahimi, P. Le Fèvre, et al., Phys. Rev. Lett. **105**, 087001 (2010).
- ⁷⁸ V. Vildosola, L. Pourovskii, R. Arita, S. Biermann, and A. Georges, Phys. Rev. B **78**, 064518 (2008).
- ⁷⁹ D. Pines, *Elementary excitations in solids : lectures on phonons, electrons, and plasmons* (W.A. Benjamin, 1964).
- ⁸⁰ Y. Nomura, M. Kaltak, K. Nakamura, C. Taranto, S. Sakai, A. Toschi, R. Arita, K. Held, G. Kresse, and M. Imada, Phys. Rev. B **86**, 085117 (2012).
- ⁸¹ K. Steiner, Y. Nomura, and P. Werner, Phys. Rev. B **92**, 115123 (2015).
- ⁸² We note that an orbital-dependent double-counting in the Around Mean Field spirit has been proposed⁵¹ and provided good agreement with the experiment for a compound with two correlated shells⁵⁰, including for the position of non-correlated bands.